Nuclear Science and Techniques (2023) 34:187
https://doi.org/10.1007/s41365-023-01339-4

Progress of photonuclear cross sections for medical radioisotope production at the SLEGS energy domain

Xuan Pang[1] · Bao-Hua Sun[1] · Li-Hua Zhu[1] · Guang-Hong Lu[1] · Hong-Bo Zhou[1] · Dong Yang[2,3]

Received: 19 July 2023 / Revised: 30 August 2023 / Accepted: 13 September 2023 / Published online: 30 November 2023

Abstract
Photonuclear reactions using a laser Compton scattering (LCS) gamma source provide a new method for producing radioisotopes for medical applications. Compared with the conventional method, this method has the advantages of a high specific activity and less heat. Initiated by the Shanghai Laser Electron Gamma Source (SLEGS), we conducted a survey of potential photonuclear reactions, (γ, n), (γ, p), and (γ, γ′) whose cross sections can be measured at SLEGS by summarising the experimental progress. In general, the data are rare and occasionally inconsistent. Therefore, theoretical calculations are often used to evaluate the production of medical radioisotopes. Subsequently, we verified the model uncertainties of the widely used reaction code TALYS−1.96, using the experimental data of the ^{100}Mo(γ, n)^{99}Mo, ^{65}Cu(γ, n)^{64}Cu, and ^{68}Zn(γ, p)^{67}Cu reactions.

Keywords Medical radioisotope · Photonuclear reaction · LCS · Cross section

1 Introduction

Radioisotopes are widely used for the diagnosis and therapy of different diseases owing to their nuclear-physical properties [1, 2]. Diagnostic radioisotopes can provide functional and metabolic information for the early treatment of diseased regions that have not yet undergone morphological or structural changes. Currently, positron emission tomography (PET) [3] and single-photon emission computed tomography (SPECT) [4] are the two major diagnostic techniques. Short-lived β$^+$-emitting radioisotopes are often used for PET. Typical examples include ^{11}C, ^{13}N, ^{15}O, and ^{18}F, which have half-lives of 20, 10, 2, and 110 min, respectively. For SPECT, γ-ray-emitting radioisotopes are frequently used, of which ^{99m}Tc with a half-life of 6 h [5] is the most common radioisotope tracer. Therapeutic radioisotopes can be combined with targeted drugs to achieve the precise removal of small diseased regions without excessive doses to normal tissues. Therefore, radioisotopes that emit low-range highly ionising radiation are of significant interest. The β$^-$-particle-emitting radioisotopes (e.g. ^{32}P, ^{89}Sr, ^{90}Y, ^{131}I, ^{177}Lu, and ^{188}Re), Auger electron cascades (e.g. ^{103}Pd and ^{125}I), and α-particle-emitting radioisotopes (e.g. ^{211}At, ^{212}Bi, ^{223}Ra, ^{225}Ac, and ^{227}Th), with a high linear energy transfer in tissue, are suitable for therapy.

More than 40 million nuclear medicine procedures are performed annually, and the demand for radioisotopes is increasing by 5% annually [6]. Currently, the production of medical radioisotopes relies primarily on nuclear reactors and cyclotrons. Thermal neutron-induced fission produces neutron-rich radioisotopes in nuclear reactors. The advantage of this method is the possibility of producing high levels of total and specific activities. However, the production of desired radioisotopes is accompanied by a considerable amount of long-lived radioactive waste, which raises numerous safety and security concerns. In addition, many nuclear reactors used for medical radioisotope production are more

This work was supported by the National Key R &D Program of China (No. 2022YFA1602401), the National Natural Science Foundation of China (Nos. 11961141004, U1832211, 11922501, 12325506) and the National Basic Science Data Center 'Medical Physics DataBase' (No. NBSDC-DB-23).

✉ Bao-Hua Sun
bhsun@buaa.edu.cn

Li-Hua Zhu
zhulh@buaa.edu.cn

[1] School of Physics, Beihang University, Beijing 100191, China

[2] College of Physics, Jilin University, Changchun 130012, China

[3] National Basic Science Data Center, Beijing 100190, China

than 50 years old and may be shut down in the near future [7]. For example, a vast majority of reactors producing ^{99}Mo are expected to shut down by 2030. Compared with reactors, cyclotrons typically produce neutron-deficient radioisotopes by charged particle reactions accompanied by less radioactive waste. In addition, they have the advantage of being more compact, allowing their placement near hospitals, and making them a useful tool for producing radioisotopes with short half-lives that range from several minutes to hours.

Another promising method for radioisotope production involves photonuclear reactions, mainly including (γ, n), (γ, p), and (γ, γ'). This is considered an alternative to radioisotope production in reactors and cyclotrons or the only method of production for certain radioisotopes. (γ, n) reactions can produce β^+-emitting radioisotopes for PET imaging, such as ^{11}C, ^{13}N, ^{15}O, and ^{18}F. These radioisotopes are produced by cyclotron-based (p, n) or (p, γ) reactions. (γ, p) reactions are suitable for producing β^--emitting radioisotopes that are currently mostly produced in reactors. High-intensity γ beams are required to obtain adequate yield using this method. With the development of laser Compton scattering (LCS) gamma sources, the production of radioisotopes via photonuclear reactions has attracted considerable attention [8–17].

In contrast to conventional bremsstrahlung gamma sources based on electron linear accelerators, LCS gamma sources have the advantages of a high photon flux and excellent monochromaticity. The advantages of photonuclear reactions using LCS gamma sources for radioisotope production are as follows:

- Differing from bremsstrahlung gamma sources, the LCS gamma sources significantly reduce the heat per useful reaction rate as its γ rays in the energy range of interest are not accompanied by an intense low-energy tail. Moreover, the LCS gamma sources have the ability to selectively tune photons to energies of interest. A high specific activity can be achieved by matching the photon energy to the giant dipole resonance (GDR) peak.
- Differing from the charged-particle induced reactions, the photonuclear reactions generate less heat as their energy deposition in targets via gamma–matter interactions is significantly smaller. Thus, the target can be thicker and requires considerably less cooling [9]. Moreover, the photonuclear reactions have the capability to simultaneously irradiate multiple targets. In this manner, it can maximise the utilisation of γ beams and produce multiple radioisotopes simultaneously [8].

The Shanghai Laser Electron Gamma Source (SLEGS) employs the LCS technique. It can generate γ beams ranging from 0.25 to −21.7 MeV with a full-spectrum flux of $10^5 - 10^7 s^{-1}$ [18] and the best possible bandwidth of γ beams of 5%–15% after passing through a dual collimation system [19]. Using collimation technology, the size of an γ beam can be continuously adjusted to within Φ25 mm [20]. The monochromaticity and high intensity of γ beams combined with detector spectrometers can be used to measure the photonuclear reaction cross section [21–24]. One of the main topics of SLEGS is the measurement of the key photonuclear reaction cross section relevant for medical radioisotope investigations, providing crucial nuclear data for the photonuclear method.

In this study, we aim to estimate the production of medical radioisotopes in the energy range of 0.25−21.7 MeV in the SLEGS domain. The remainder of this paper is organised as follows. In Sect. 2, we summarise the radioisotopes that can be produced via (γ, n), (γ, p), and (γ, γ') reactions and discuss their experimental feasibility. Owing to the scarcity of cross-sectional data regarding photonuclear reactions, theoretical calculations are often used to assess the yields of medical radioisotopes. In Sect. 3, the cross-sectional data of the ^{100}Mo(γ, n), ^{65}Cu(γ, n), and ^{68}Zn(γ, p) reactions in the SLEGS energy region were investigated to produce ^{99}Mo, ^{64}Cu, and ^{67}Cu radioisotopes. Finally, we provide a summary in Sect. 4.

2 Medical radioisotopes produced in photonuclear reactions

In this section, we discuss potential (γ, n), (γ, p), and (γ, γ') reactions for the production of medical radioisotopes. Crucial considerations include the natural abundance of the target isotopes, half-life of the radioisotopes, and available experimental data. Generally, it is preferable to have a target isotope with a dominant abundance (*e.g.* , greater than 10%) and a suitable half-life (several tens of minutes to days) for the produced radioisotope. However, the lack of experimental data may limit the medical applications of radioisotopes.

Different methods are available for measuring photonuclear reactions, including in-beam and offline measurements. Four π ^{3}He neutron detection arrays, charged particle detectors, and nuclear resonance fluorescence spectrometers are commonly used for in-beam measurements of (γ, n), (γ, p), and (γ, γ') reactions. Offline measurement is suitable for determining all three types of photonuclear reactions only in cases where the residual decay has an unambiguous γ-ray and the lifetime of the residual nucleus is within a range of minutes to hours.

2.1 (γ, n) reactions

Radioisotopes can be most efficiently produced by exciting the target nuclide into a GDR using photons. The GDR is characterised by a large peak cross section and

broad width, resulting in a large integral cross section. The shape of the GDR follows a Lorentzian distribution with a spreading width of approximately 5 MeV [25–27]. Generally, a considerable portion of the total photonuclear cross section is known to originate from the (γ, n) reactions, which increases as the charge number of the target nuclide increases, making the following chemical separation easier. For example, the ^{100}Mo(γ, n) reaction accounts for more than 70% of the total photonuclear reactions within the energy range of 8.4–15 MeV. Therefore, medium- and heavy-mass nuclei are ideal for production via (γ, n) reactions [28].

Table 1 summarises the 15 medical radioisotopes produced by (γ, n) reactions [8, 14, 29–31]. Excluding ^{100}Mo, the natural abundance of these reaction targets exceeds 10%. A higher natural abundance results in a higher yield and lower impurity content. The seventh column indicates the current status of the EXFOR database [32]. The experimental data for only nine radioisotopes are presented in Appendix. Among these, the ^{19}F(γ, n) reaction has only one dataset that was measured in the 1960 s. The data for the ^{90}Zr(γ, n), ^{100}Mo(γ, n), and ^{187}Re(γ, n) reactions do not cover the entire GDR energy region. There is a significant discrepancy between the two sets of data for the ^{65}Cu(γ, n) reaction: It is possible to determine the relevant cross sections at SLEGS.

2.2 (γ, p) reactions

Despite the nucleus being excited beyond the proton separation energy of the photons, it does not necessarily lose a proton. Only for excitations well beyond the proton separation energy, the proton can acquire sufficient kinetic energy to effectively cross the Coulomb barrier. However, in these cases, the excitation energy typically exceeds the separation energies of one or two neutrons. Therefore, the neutron emission channel competes with the proton emission channel. For light and certain medium-mass nuclei, the cross sections of the (γ, p) reactions are comparable to and occasionally exceed those of the (γ, n) reactions, owing to the shell structure of the nuclei. Certain heavier β$^-$ emitters for radionuclide therapy can also be produced by (γ, p) reactions, but the increasing Coulomb barrier leads to the production of small cross sections. (γ, p) reactions result in the daughter and parent isotopes being chemically different. Several advanced chemical-separation techniques have been developed for this purpose. For example, a simple and reproducible three-ion exchange matrix approach was developed to

Table 1 Medical radioisotope ^{A}X production via the $^{A+1}X(\gamma, n)^{A}X$ reactions [8, 14, 29–31].

^{A+1}X	Nat. abu. (%)	^{A}X	$T_{1/2}$	Decay mode	E_{th} (MeV)	EXFOR data	Medical application	Exp. method	γ-ray (keV)
^{12}C	98.93	^{11}C	20.364 m	%ε = 100	18.7	Yes	PET	*a*;*b*	511
^{14}N	99.63	^{13}N	9.965 m	%ε = 100	10.5	Yes	PET	*a*;*b*	511
^{16}O	99.757	^{15}O	122.24 s	%ε = 100	15.6	Yes	PET	*a*	–
^{19}F	100	^{18}F	109.77 m	%ε = 100	10.4	Yes	PET	*a*;*b*	511
^{45}Sc	100	^{44}Sc	3.97 h	%ε = 100	11.3	No	PET	*a*;*b*	511;1157
^{63}Cu	69.15	^{62}Cu	9.673 m	%ε = 100	10.8	Yes	PET	*a*;*b*	511
^{65}Cu	30.85	^{64}Cu	12.7 h	%ε = 61.5 %β$^-$ = 38.5	9.91	Yes	PET;Radiotherapy	*a*;*b*	511
^{69}Ga	60.108	^{68}Ga	67.71 m	%ε = 100	10.3	No	PET	*a*;*b*	511;1077
^{90}Zr	51.45	^{89}Zr	78.41 h	%ε = 100	11.9	Yes	PET	*a*	–
^{100}Mo	9.82	^{99}Mo	65.976 h	%β$^-$ = 100	8.29	Yes	SPECT	*a*;*b*	740;778
^{104}Pd	11.14	^{103}Pd	17.0 d	%ε = 100	10.0	No	Radiotherapy	*a*	–
^{166}Er	33.503	^{165}Er	10.36 h	%ε = 100	8.47	No	Radiotherapy	*a*	–
^{170}Er	14.91	^{169}Er	9.4 d	%β$^-$ = 100	7.25	No	Radiotherapy	*a*	–
^{187}Re	62.60	^{186}Re	3.7 d	%β$^-$ = 92.53 %ε = 7.47	7.36	Yes	SPECT;Radiotherapy	*a*	–
^{193}Ir	62.70	^{192}Ir	73.8 d	%β$^-$ = 95.24 %ε = 4.76	7.77	No	Radiotherapy	*a*	–

The natural abundance of ^{A+1}X is provided. The produced medical radioisotopes ^{A}X are characterised by the half-lives $T_{1/2}$ and decay modes. Here, %ε represents the probabilities of nuclear decay via electron capture or β$^+$ decay. %β$^-$ represents the probabilities of β$^-$ decay. E_{th} represents the threshold energy of the reaction. The seventh column indicates whether the $^{A+1}X(\gamma, n)^{A}X$ reactions have experimental data in the EXFOR database [32]. *a* and *b* indicate that the radioisotope can be studied by in-beam and off-line measurements, respectively. The last column presents the probable γ-rays of interest in the offline measurement. The data are obtained from Ref. [33]

Table 2 Same as Table 1 but for medical radioisotopes ^{A}X production via the $^{A+1}Y(\gamma, p)^{A}X$ reactions [8, 38–40].

^{A+1}Y	Nat. abu. (%)	^{A}X	$T_{1/2}$	Decay mode	E_{th} (MeV)	EXFOR data	Medical application	Exp. method	γ-ray (keV)
^{44}Ca	2.09	^{43}K	22.3 h	$\%\beta^- = 100$	12.1	Yes	Radiotherapy	*a*;*b*	373;617
^{48}Ti	73.72	^{47}Sc	3.35 d	$\%\beta^- = 100$	11.4	No	Radiotherapy	*a*	–
^{58}Ni	68.077	^{57}Co	271.74 d	$\%\varepsilon = 100$	8.17	No	Radiotherapy	*a*	–
^{68}Zn	18.45	^{67}Cu	61.83 h	$\%\beta^- = 100$	9.97	Yes	Radiotherapy	*a*;*b*	861;2502
^{91}Zr	11.22	^{90}Y	64.053 h	$\%\beta^- = 100$	8.68	No	Radiotherapy	*a*	–
^{106}Pd	27.33	^{105}Rh	35.36 h	$\%\beta^- = 100$	9.34	No	Radiotherapy	*a*;*b*	319
^{112}Sn	0.97	^{111}In	2.805 d	$\%\varepsilon = 100$	7.55	No	SPECT;Radiotherapy	*a*	–
^{132}Xe	26.9	^{131}I	8.025 d	$\%\beta^- = 100$	9.12	No	Radiotherapy	*a*	–
^{162}Dy	25.475	^{161}Tb	6.89 d	$\%\beta^- = 100$	8.00	No	SPECT;Radiotherapy	*a*	–
^{167}Er	22.869	^{166}Ho	26.824 h	$\%\beta^- = 100$	7.50	No	SPECT;Radiotherapy	*a*	–
^{178}Hf	27.28	^{177}Lu	6.647 d	$\%\beta^- = 100$	7.34	Yes	SPECT;Radiotherapy	*a*;*b*	208
^{189}Os	16.15	^{188}Re	17 h	$\%\beta^- = 100$	7.25	No	SPECT;Radiotherapy	*a*	–

Nat. abu. indicates the natural abundance of ^{A+1}Y. The seventh column indicates whether experimental data regarding the $^{A+1}Y(\gamma, p)^{A}X$ reactions are available in the EXFOR database [32]

separate ^{67}Cu from ^{68}Zn [34]. Separation techniques exist for other pairs, such as Ti/Sc, Zr/Y, and Hf/Lu [35–37].

The potential (γ, p) reactions used for nuclear medicine are listed in Table 2. However, the experimental data regarding this topic are scarce. Only limited data for ^{43}K, ^{67}Cu, and ^{177}Lu have been obtained by using the bremsstrahlung gamma source, as detailed in Appendix. No error bars are shown for the ^{43}K data, whereas relatively large errors ranging from typically 10% to 100% for ^{67}Cu and ^{177}Lu have been demonstrated.

2.3 (γ, γ') reactions

A nuclear isomer is the metastable state of an atomic nucleus, in which one or more nucleons (protons or neutrons) occupy higher energy levels than the ground state of the same nucleus. The lifetime and excitation energy are two important properties of nuclear isomers. The excitation energy between the isomer and ground state is characteristic and can be used to identify nuclides. Nuclear isomers can be deexcited by the emission of γ rays and/or the conversion of electrons to the ground state. The γ-emitting isomers can be used as radioactive labels for SPECT imaging. Nuclear isomers-emitting low-energy Auger electrons are potential radioisotopes for targeted therapy.

Conventional production methods, such as (n, γ) reactions, have relatively low yields because the dominant part of the production proceeds directly to the nuclear ground state with a spin closer to that of the target isotope. Using monochromatic and small-bandwidth LCS photons, transitions from a stable or long-lived nuclear ground state to higher energy levels can be selectively excited. Such levels serve as gateway states, which then partially decay to the isomeric state directly or via a cascade. The (γ, γ') reaction

Table 3 Same as Table 1 but for medical isomers ^{Am}X production via the $^{A}X(\gamma, \gamma')^{Am}X$ reactions [8, 13].

^{A}X	Nat. abu. (%)	^{Am}X	$T^{m}_{1/2}$	E_m/E_{th} (keV)	Decay mode	EXFOR data	Medical application
^{103}Rh	100	^{103m}Rh	56.114 m	39.8	$\%IT = 100$	Yes	Radiotherapy
^{113}In	4.29	^{113m}In	99.476 m	391.7	$\%IT = 100$	Yes	SPECT;Radiotherapy
^{115}In	95.71	^{115m}In	4.486 h	336.2	$\%IT = 95$	Yes	SPECT;Radiotherapy
					$\%\beta^- = 5$		
^{117}Sn	7.68	^{117m}Sn	13.76 d	314.6	$\%IT = 100$	No	Radiotherapy
^{176}Lu	2.599	^{176m}Lu	3.664 h	122.8	$\%\beta^- = 99.90$	No	Radiotherapy
					$\%\varepsilon = 0.09$		
^{195}Pt	33.78	^{195m}Pt	4.01 d	259.3	$\%IT = 100$	Yes	Radiotherapy

The isomeric states ^{Am}X are characterised by the energy E_m, half-lives $T^{m}_{1/2}$, and decay modes. Here, $\%IT$ represents the probabilities of nuclear decay via isomeric transitions. E_{th} equals E_m. The seventh column indicates whether the $^{A}X(\gamma, \gamma')^{Am}X$ reactions have experimental data in the EXFOR database [32]. $^{A}X(\gamma, \gamma')^{Am}X$ reactions can be investigated by off-line measurements where the γ-ray energy of interest is equal to E_m

is equivalent to storing the energy of an incident photon in an isotope that acts as a container.

Table 3 lists the six isomers that can be produced by (γ, γ') reactions for medical applications. Excluding ^{117m}Sn and ^{176m}Lu, the experimental data for the other radioisotopes are detailed in Appendix. The dataset of ^{103m}Rh did not have error bars, and two different results were reported from 6 to 23 MeV. For ^{113m}In, two cross-sectional datasets differ by more than 300 times at 8 MeV. For ^{115m}In, there were significant discrepancies between multiple datasets. The data of ^{195m}Pt have a large relative error as high as 100% at 3.5, 7.5, and 8 MeV.

3 Evaluation of cross sections for ^{99}Mo, ^{64}Cu, and ^{67}Cu production

The cross-section data were used to calculate the expected yield of the radioisotopes for a given thickness and enrichment of the target material, and to determine the optimum energy range for the production of the desired radioisotope and the level of radioisotopic impurities. However, the slow development of gamma sources and small cross sections of photonuclear reactions resulted in a relatively small number of experimental studies regarding this cross-sectional data. There is often scattering between different experimental datasets. As a result, the cross sections predicted by the theoretical models play a key role in the production of medical radioisotopes.

The TALYS code [41] offers a unified approach for calculating nuclear reactions that involve neutrons, photons, protons, deuterons, tritons, ^{3}He, and α particles in the keV–200 MeV energy range and for target nuclides with masses of 5 and 339. The code outputs a set of reaction data, *for example* cross sections, energy spectra, and angular distributions of the emitted particles, etc. Numerous studies have tested the TALYS code and demonstrated that it has reliable predictive power in terms of the nuclear reaction calculations [42–44]. In the TALYS code, the decay of the compound nuclear state from the photonuclear reaction was treated using the Hauser-Feshbach (HF) statistical model [45]. The nuclear-level density and γ strength function were the main input parameters. In this study, we adapted the TALYS−1.96 code. It implemented six different nuclear level density (NLD) models and nine different models of γ strength functions (γSF), as shown in Table 4. The NLD and γSF models employ phenomenological and microscopic approaches, respectively.

In this section, we select the ^{99}Mo, ^{64}Cu, and ^{67}Cu radioisotopes as examples to compare the model calculations with the experimental data. ^{99m}Tc decayed by ^{99}Mo is the most frequently used radioisotope in nuclear medicine. ^{68}Zn is of interest owing to its applications in the production of the medical radioisotope ^{67}Cu; ^{67}Cuand ^{64}Cu can form a "matched pair" [46, 47]. Therapeutic ^{67}Cu, along with positron-emitting ^{64}Cu, can measure the uptake kinetics in an organ of a patient by PET imaging, allowing for a precise dosimetric calculation. We used the default values of NLD and the γSF models in the following calculations.

3.1 ^{99}Mo/^{99m}Tc

With half-lives of 6 h and 140 keV γ-rays, ^{99m}Tc is nearly ideal for SPECT imaging. The most common method

Table 4 The descriptions of NLD and γSF models in the TALYS−1.96 code

Input parameter	Detailed description
ldmodel 1 (default)	Constant temperature + Fermi gas model
ldmodel 2	Back-shifted Fermi gas model
ldmodel 3	Generalised superfluid model
ldmodel 4	Skyrme-Hartree-Fock-Bogoliubov level densities from numerical tables
ldmodel 5	Gogny-Hartree-Fock-Bogoliubov (GHFB) level densities from numerical tables
ldmodel 6	Temperature-dependent GHFB level densities from numerical tables
Strength 1 (default for incident neutrons)	Kopecky-Uhl generalsed Lorentzian
Strength 2 (default for other incident particles)	Brink-Axel Lorentzian
Strength 3	Hartree-Fock + Bardeen-Cooper-Schrieffer (BCS) tables
Strength 4	Hartree-Fock-Bogoliubov (HFB) tables
Strength 5	Goriely's hybrid model
Strength 6	Goriely temperature-dependent HFB model
Strength 7	Temperature-dependent relativistic mean field (RMF) model
Strength 8	Gogny D1M HFB + quasiparticle random phase approximation (QRPA)
Strength 9	Simplified modified Lorentzian (SMLO) model

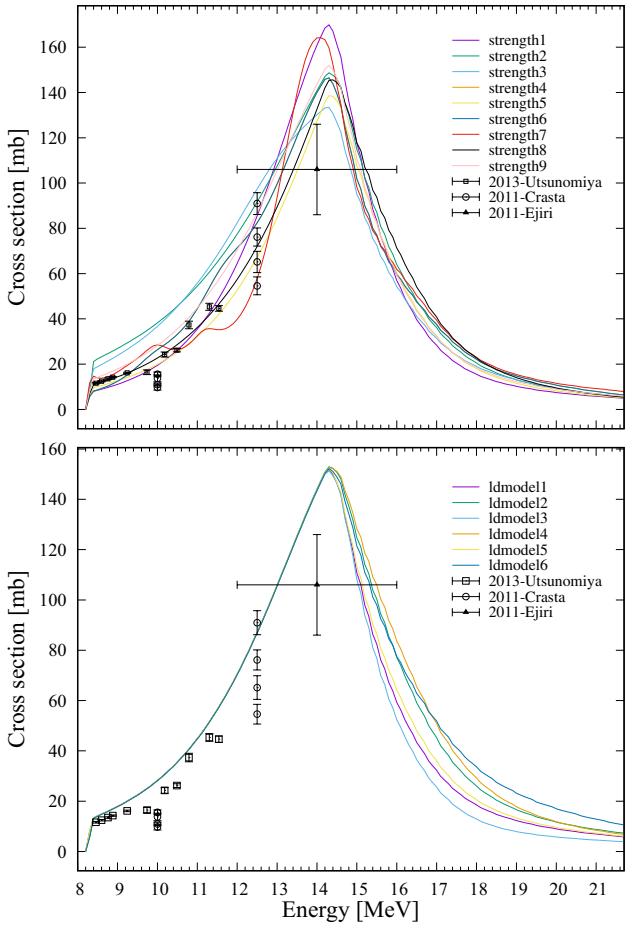

Fig. 1 (Color online) ^{100}Mo$(\gamma, n)^{99}$Mo reaction cross sections

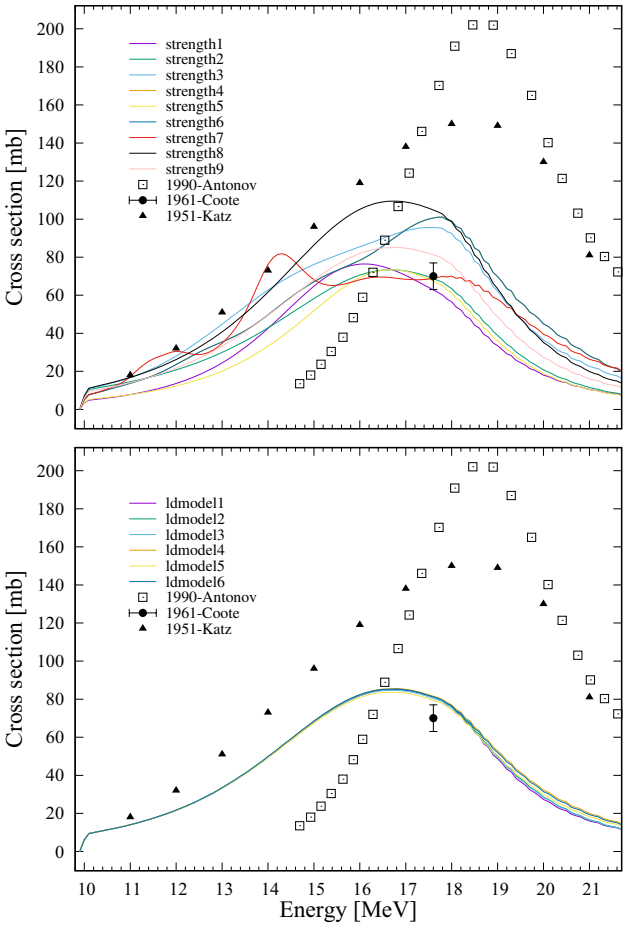

Fig. 2 (Color online) ^{65}Cu$(\gamma, n)^{64}$Cu reaction cross sections

to obtain ^{99m}Tc is by elution from ^{99}Mo generators. The ^{100}Mo(γ, n) reaction has a sufficient potential to produce ^{99}Mo. The excitation functions are presented in Fig. 1, which covers the entire GDR energy range. The cross sections of ^{100}Mo$(\gamma, n)^{99}$Mo were experimentally measured by Utsunomiya et al. [48], Crasta et al. [49], and Ejiri et al. [14]. The gamma sources used in the experiments were LCS and bremsstrahlung. All the experimental results were distributed in the low-energy region of the GDR and did not exceed the peak. Figure 1 demonstrates that the shape and value of the excitation function are highly sensitive to the choice of the γSF model, particularly at the peak position of GDR. Excluding strength 2 and 3, the remaining γSF models yield relatively similar results that are close to the experimental results. Different γSF models produce similar predictions for energies above the GDR peak. Overall, the cross sections estimated using Strength 8 achieve the best agreement with the experimental data. As shown in Fig. 1, the calculation results of all the NLD models below the peak are consistent but significantly higher than the experimental data, whereas those above the peak are significantly different. The data predicted by the models at energies above 14 MeV are highly valuable. New experiments can be conducted based on SLEGS to verify the model predictions.

3.2 ^{64}Cu

As listed in Table 1, the decay characteristics of ^{64}Cu render it useful for nuclear medicine [50]. It combines PET diagnostic capabilities with those of radiotherapy, with average electron emissions of 190 keV. Currently, ^{64}Cu is mainly produced by small cyclotrons through ^{64}Ni(p, n) reactions [51–54]. Alternative production using ^{65}Cu(γ, n) does not require rare or expensive ^{64}Ni targets and simplifies the chemical separation step. The experimental data for the cross sections of the ^{65}Cu$(\gamma, n)^{64}$Cu reaction are presented in Fig. 2 along with the TALYS. The measurements by Katz et al. [55] and Antonov et al. [56] were performed using bremsstrahlung gamma sources. However, they differed significantly in terms of their shape and value. Coote et al. [57] obtained a single cross section at 17.6 MeV using

monochromatic γ-rays from the ^{7}Li(p, γ)^{8}Be reaction. The cross section is consistent with the calculation but lower than other experimental data by 80 to 120 mb. The cross sections of ^{65}Cu(γ, n)^{64}Cu can significantly vary with the choice of the γSF models but not the NLD models. However, the discrepancies between the experiments and models cannot be compensated for by varying the γSF models. Future experiments regarding the ^{65}Cu photoneutron reaction using a monochromatic LCS gamma source will be useful for resolving these discrepancies and provide assurance for its medical applications.

3.3 ^{67}Cu

^{67}Cu is a promising β^{-}-particle emitter with an average energy of 141 keV for the targeted radiotherapies. The size of these particles in the tissue was of the same order as the cell diameter. This reduces the unwanted dose burden on patients [58]. With a half-life of 61.83 h and low energy γ emissions (91.266 keV, 7%; 93.311 keV, 16.1%; 184.577 keV, 48.7%), ^{67}Cu can provide a long therapeutic effect. ^{67}Cu and its stable daughter ^{67}Zn are nontoxic to the body, and both Cu and Zn are prevalent trace elements in the body. Along with the PET imaging radioisotope ^{64}Cu, it forms a "matched pair." However, the widespread clinical use of ^{67}Cu-based radiopharmaceuticals has been limited by their availability, quantity, and quality. Experiments [59–63] have shown that the ^{68}Zn(γ, p) reaction has the potential to produce sufficient quantities of ^{67}Cu with a sufficient purity for medical use. Moreover, various Cu and Zn separation methods have been employed in radiochemical processing [34, 64–66].

Figure 3 presents the excitation function of the ^{68}Zn(γ, p)^{67}Cu reaction. Experimental data regarding this reaction are scarce, with only one group of two points in the energy region of SLEGS [67]. The data are significantly inconsistent with any calculation and hardly constrain NLD and γSF models. In contrast to the (γ, n) reaction of several hundred mb, the (γ, p) reaction is typically several mb in the medium-heavy nuclei. Additionally, protons can easily stop at the target and are difficult to detect. If the product nuclei of the (γ, p) reaction are unstable and have a moderate half-life, the cross sections can be determined by offline measurements of the characteristic γ-rays during decay. For the ^{68}Zn(γ, p) reaction, an offline measurement technique can be employed to determine its cross sections.

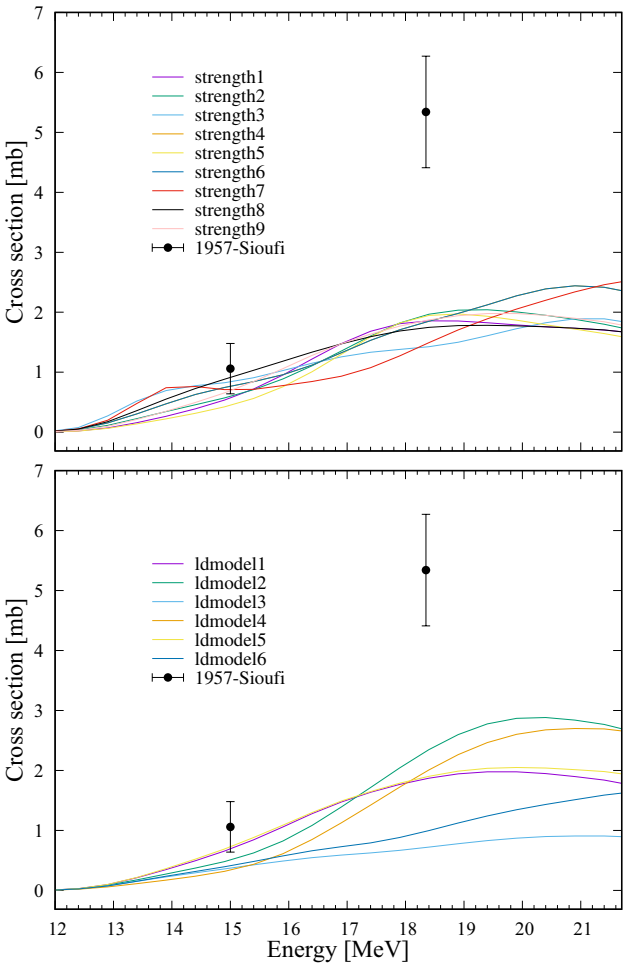

Fig. 3 (Color online) ^{68}Zn(γ, p)^{67}Cu reaction cross sections

4 Summary

In this study, we summarise the medical radioisotopes that can be produced by (γ, n), (γ, p), and (γ, γ′) reactions, along with the experimental data for these production pathways. We investigated the photonuclear reaction cross sections for the production of ^{99}Mo, ^{64}Cu, and ^{67}Cu. The experimental data for ^{99}Mo and ^{67}Cudid not cover the entire GDR energy region, whereas the data for ^{64}Cu exhibited a significant discrepancy. To better constrain the NLD and γSF models in TALYS, additional experimental measurements at SLEGS in the energy region of GDR are necessary in the future.

To compare the productivity of the photonuclear method with that of traditional methods, we consider the production of ^{99}Mo/^{99m}Tc as an example. The highest flux currently available for SLEGS is $10^7 s^{-1}$. We adopted the calculated results by the TALYS−1.96 code using the Strength 8 model for the yield calculations, which provided a maximum of 145 mb of the ^{100}Mo(γ, n) reaction cross section at the incident photon energy of 14.4 MeV. After irradiating a $^{100}MoO_3$ target with a radius of 2 mm and a thickness of 1 cm for 5 times the half-life of ^{99}Mo, the saturation specific activity of ^{99}Mo and ^{99m}Tc can reach 4.76 and 4.74 μCi/g, respectively. The use of stacked targets can further enhance production. When the energy regions corresponding to the maximum cross sections of the targeted nuclear reactions are close, multiple radioisotopes can be simultaneously produced. For example, the ^{62}Cu, ^{64}Cu, and ^{89}Zr radioisotopes can be produced simultaneously when the incident photon energy is approximately 17 MeV.

Currently, ^{99}Mo is primarily produced by the (n, f) reaction in a high-flux reactor using an enriched ^{235}U target. The specific activity of ^{99}Mo can reach 185 TBq/g (5000 Ci/g) [6]. However, most reactors will gradually shut down by 2030 [68]. Medical cyclotrons can be used to directly generate ^{99m}Tc via the ^{100}Mo(p, 2n) reaction. According to the experimental data, an enriched ^{100}Mo target irradiated with a 16.5-MeV proton beam at 130 μA for 6 h yielded 116 GBq/g (3.13 Ci/g) of ^{99m}Tc [69]. Recently, a subcritical ^{99}Mo production system was developed, which is driven by an accelerator-based deuterium–deuterium (D–D) neutron source. The D–D fusion reaction generates neutrons that irradiate a low-enriched uranium solution and induce fission in ^{235}U. The system can generate 47.8 mCi/g ^{99}Mo for a stable 24-h operation with a neutron intensity of 1×10^{14} n/s [70]. Bremsstrahlung gamma sources based on linear electron accelerators are often used to produce ^{99}Mo radioisotopes. Using a $^{100}MoO_3$ target irradiate with a 35-MeV electron beam at 100 μA for 20 h, the specific activity can achieve 4.4 GBq/g (119 mCi/g) [71]. NorthStar Medical Radioisotopes developed a ^{99}Mo production system using an electron linear accelerator. Using this system based on (γ, n) reactions, approximately 30% more ^{99}Mo is produced per gram of the target material compared with the traditional neutron capture route [72, 73].

In comparison, the specific activity produced by the photonuclear method based on SLEGS was low. With a further increase in the flux of γ beams, from $10^7 s^{-1}$ to $10^{15} s^{-1}$ [20], the specific activity of ^{99}Mo can reach up to 4×10^2 Ci/g. For the 2-day protocol, the activity of the ^{99m}Tc-labelled tracers required for one myocardial perfusion imaging was 24 mCi [74]. The total yield of stacked targets in one year can provide 400,000 myocardial perfusion images. As the flux of SLEGS increases in the future, this method is promising for producing medical radioisotopes and will become feasible in China.

Appendix

Experimental data for the production of medical radioisotopes by (γ, n), (γ, p), and (γ, γ') reactions are summarised. Table 5 lists relevant information on these reactions. All the data and information were obtained from the EXFOR database [32].

Table 5 Information regarding experimental data for the production of medical radioisotopes by photonuclear reactions

Target	Reaction	Product	Year	Gamma source	Reference
^{12}C *	(γ, n)	^{11}C	1951	Bremsstrahlung	[55]
			1957	Bremsstrahlung	[75]
			1959	$^{3}H(p,\gamma)^{4}He$	[76]
			1961	Bremsstrahlung	[77]
			1962	$^{3}H(p,\gamma)^{4}He$	[78]
			1966	Bremsstrahlung	[79]
			1966	Bremsstrahlung	[80]
			1966	$^{3}H(p,\gamma)^{4}He$	[81]
^{14}N	(γ, n)	^{13}N	1960	Bremsstrahlung	[82]
			1987	Bremsstrahlung	[83]
^{16}O *	(γ, n)	^{15}O	1962	$^{3}H(p,\gamma)^{4}He$	[78]
			1966	Bremsstrahlung	[84]
			1970	Bremsstrahlung	[85]
			1985	Bremsstrahlung	[86]
			1991	Bremsstrahlung	[87]
^{19}F	(γ, n)	^{18}F	1962	$^{3}H(p,\gamma)^{4}He$	[78]
^{63}Cu	(γ, n)	^{62}Cu	1951	Bremsstrahlung	[88]
			1951	Bremsstrahlung	[55]
			1954	Bremsstrahlung	[89]
			1955	Bremsstrahlung	[90]
			1959	$^{7}Li(p,\gamma)^{8}Be$	[91]
			1960	$^{7}Li(p,\gamma)^{8}Be$	[92]
			1961	$^{7}Li(p,\gamma)^{8}Be$	[57]
			1962	$^{3}H(p,\gamma)^{4}He$	[78]
			1968	In-flight positron annihilation	[93]
			1968	Bremsstrahlung	[94]
			1979	In-flight positron annihilation	[95]
			1984	$^{7}Li(p,\gamma)^{8}Be$	[96]
			1984	Bremsstrahlung	[97]
			2012	Bremsstrahlung	[98]
^{65}Cu *	(γ, n)	^{64}Cu	1951	Bremsstrahlung	[55]
			1961	$^{7}Li(p,\gamma)^{8}Be$	[57]
			1990	Bremsstrahlung	[56]
^{90}Zr	(γ, n)	^{89}Zr	1978	Bremsstrahlung	[99]
			2010	Bremsstrahlung	[100]
			2019	LCS	[101]
^{100}Mo	(γ, n)	^{99}Mo	1978	Bremsstrahlung	[99]
			2011	Bremsstrahlung	[49]
			2011	LCS	[14]
			2013	LCS	[48]
^{187}Re	(γ, n)	^{186}Re	2005	LCS	[102]
^{44}Ca	(γ, p)	^{43}K	1978	Bremsstrahlung	[99]
^{68}Zn	(γ, p)	^{67}Cu	1957	Bremsstrahlung	[67]
			2021	Bremsstrahlung	[56]
^{178}Hf	(γ, p)	^{177}Lu	2020	Bremsstrahlung	[103]
^{103}Rh	(γ, γ′)	^{103m}Rh	1961	Bremsstrahlung	[104]
^{113}In	(γ, γ′)	^{113m}In	2006	Bremsstrahlung	[105]
			2017	Bremsstrahlung	[106]
^{115}In	(γ, γ′)	^{115m}In	1957	Bremsstrahlung	[107]

Table 5 (continued)

Target	Reaction	Product	Year	Gamma source	Reference
			1993	Bremsstrahlung	[108]
			2001	Bremsstrahlung	[109]
			2006	Bremsstrahlung	[110]
			2017	Bremsstrahlung	[106]
			2018	LCS	[111]
^{195}Pt	(γ,γ')	^{195m}Pt	2006	Bremsstrahlung	[105]

* Experimental data within a specific energy range, instead of all of experimental data

(γ, n)

The cross-sectional data for the production of ^{11}C, ^{13}N, ^{15}O, ^{18}F, ^{62}Cu, ^{64}Cu, ^{89}Zr, ^{99}Mo, and ^{186}Re radioisotopes by (γ, n) reactions are shown in the following figures (Figs. 4, 5, 6, 7, 8, 9, 10, 11 and 12).

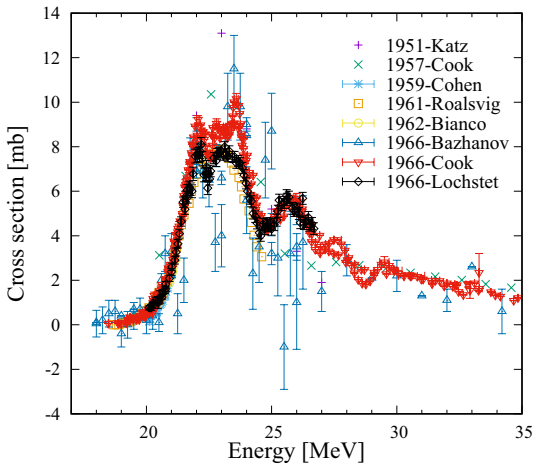

Fig. 4 (Color online) ^{12}C$(\gamma, n)^{11}$C reaction cross sections

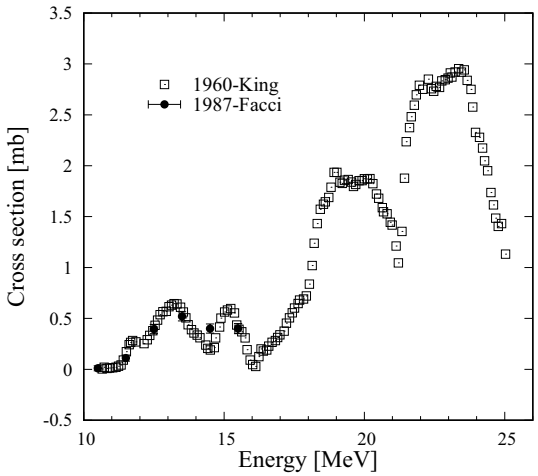

Fig. 5 ^{14}N$(\gamma, n)^{13}$N reaction cross sections

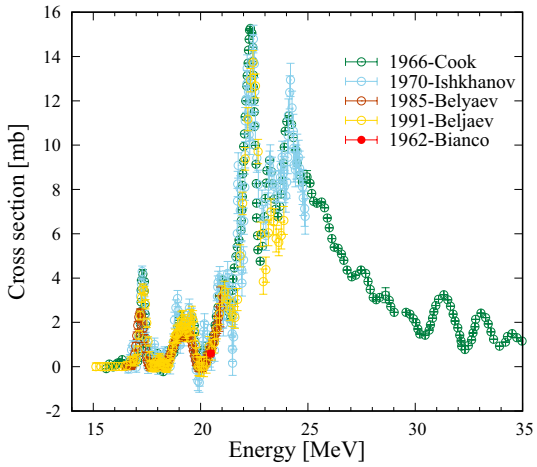

Fig. 6 (Color online) ^{16}O$(\gamma, n)^{15}$O reaction cross sections

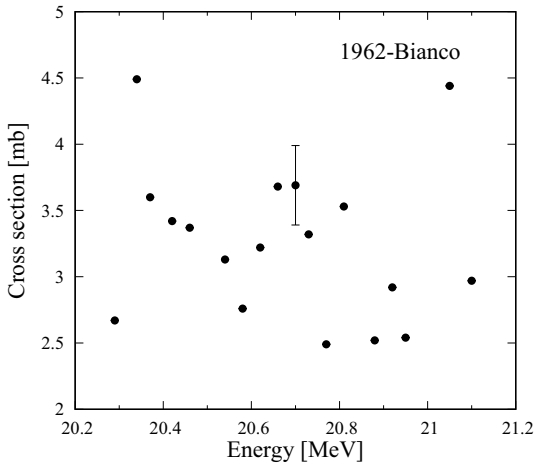

Fig. 7 ^{19}F$(\gamma, n)^{18}$F reaction cross sections

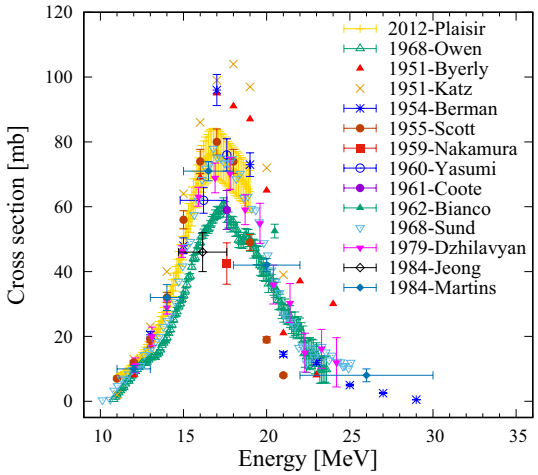

Fig. 8 (Color online) ^{63}Cu(γ, n)^{62}Cu reaction cross sections

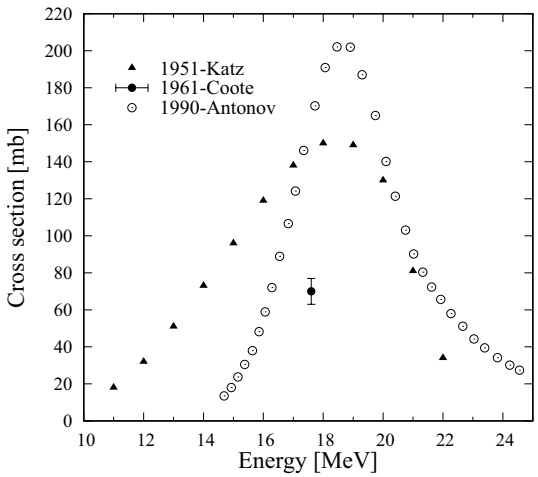

Fig. 9 ^{65}Cu(γ, n)^{64}Cu reaction cross sections

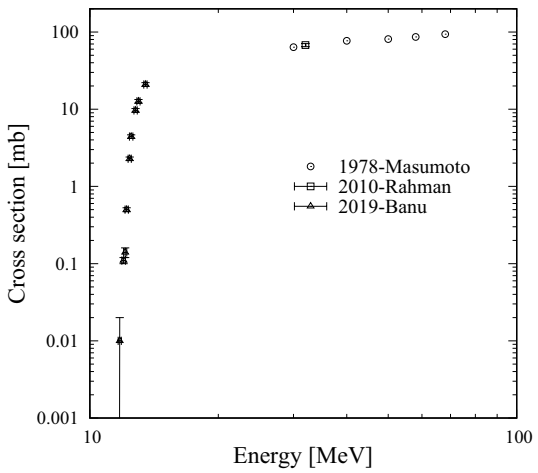

Fig. 10 ^{90}Zr(γ, n)^{89}Zr reaction cross sections

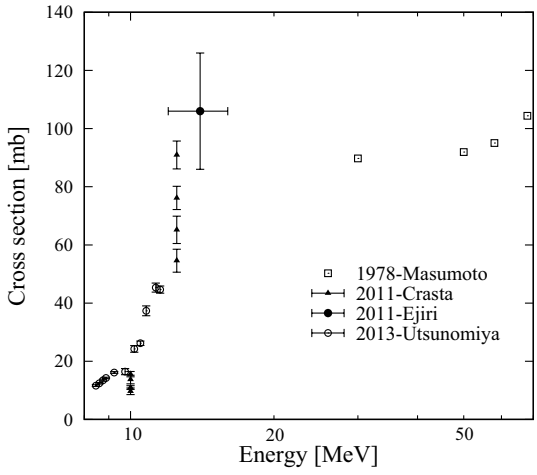

Fig. 11 ^{100}Mo(γ, n)^{99}Mo reaction cross sections

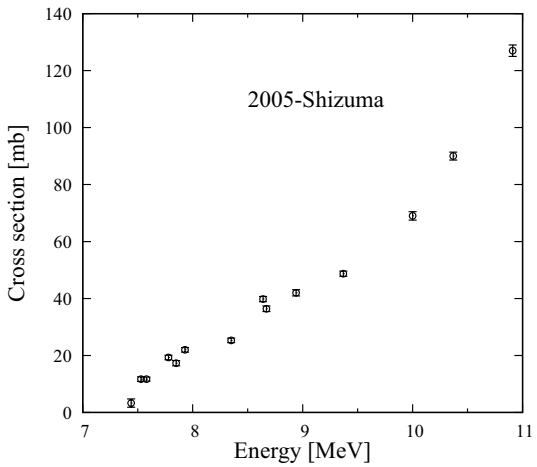

Fig. 12 ^{187}Re(γ, n)^{186}Re reaction cross sections

(γ, p)

The cross-sectional data for the production of ^{43}K, ^{67}Cu, and ^{177}Lu radioisotopes by (γ, p) reaction are shown in the following figures (Figs. 13, 14 and 15).

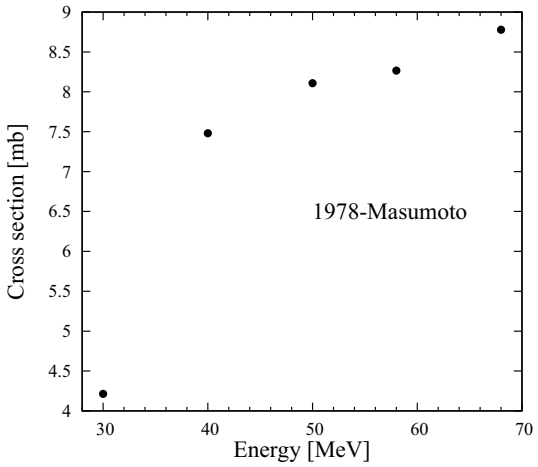

Fig. 13 $^{44}Ca(\gamma, p)^{43}K$ reaction cross sections

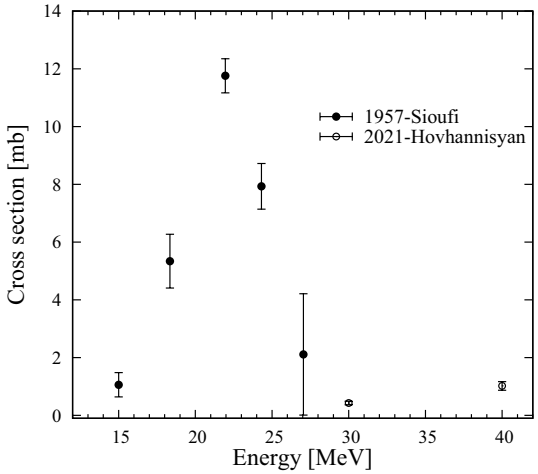

Fig. 14 $^{68}Zn(\gamma, p)^{67}Cu$ reaction cross sections

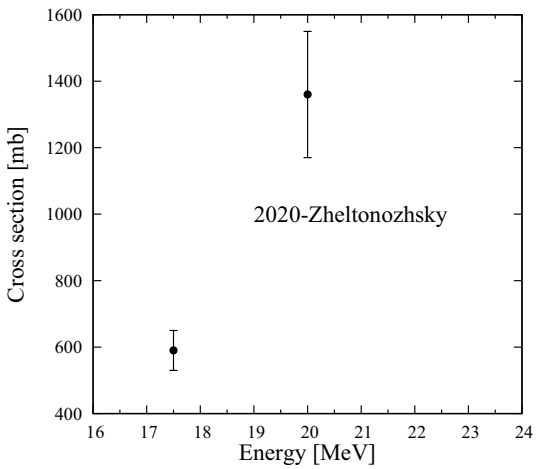

Fig. 15 $^{178}Hf(\gamma, p)^{177}Lu$ reaction cross sections

(γ, γ')

The cross-sectional data for the production of ^{103m}Rh, ^{113m}In, ^{115m}In, and ^{195m}Pt radioisotopes by (γ, γ') reaction are shown in the following figures (Figs. 16, 17, 18 and 19).

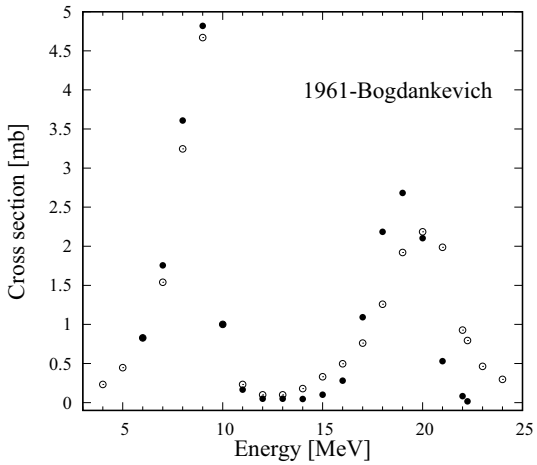

Fig. 16 $^{103}Rh(\gamma, \gamma')^{103m}Rh$ reaction cross sections

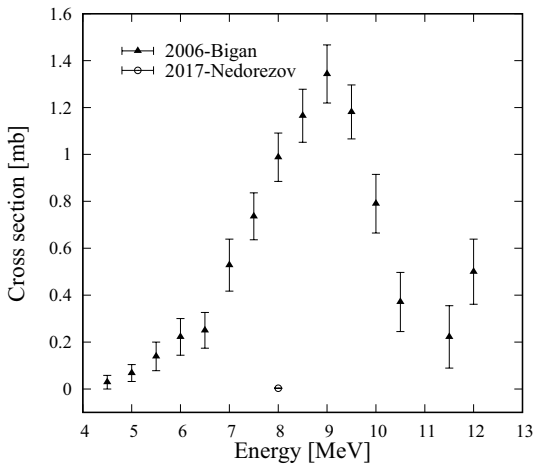

Fig. 17 $^{113}In(\gamma, \gamma')^{113m}In$ reaction cross sections

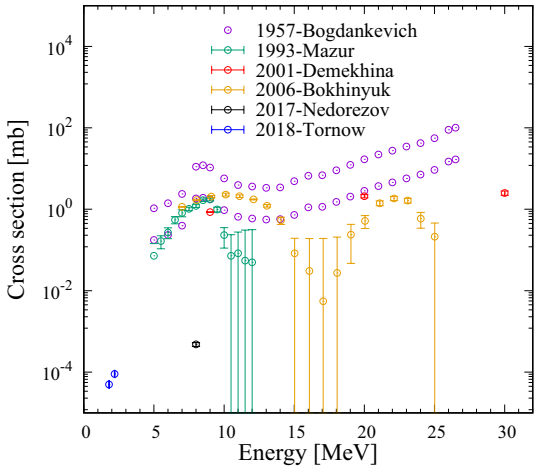

Fig. 18 (Color online) ^{115}In(γ, γ′)^{115m}In reaction cross sections

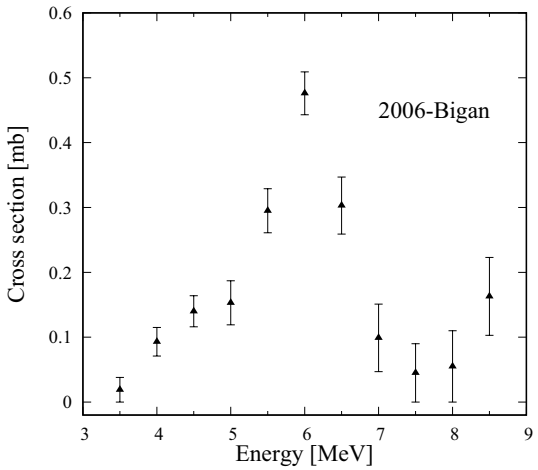

Fig. 19 ^{195}Pt(γ, γ′)^{195m}Pt reaction cross sections

Author contributions All authors contributed to the study conception and design. Material preparation, data collection and analysis were performed by Xuan Pang and Bao-Hua Sun. All authors commented on previous versions of the manuscript and read and approved the final manuscript.

Data availability The data that support the findings of this study are openly available in Science Data Bank at https://www.doi.org/10.57760/sciencedb.12006 and https://cstr.cn/31253.11.sciencedb.12006.

Declarations

Conflict of interest The authors declare that they have no competing interests.

References

1. Ch. Schiepers(ed.) *Diagnostic Nuclear Medicine* (Springer & Berlin 2006)
2. G.J.R. Cook (ed.), *Clinical Nuclear Medicine* (Hodder Arnold, London, 2006)
3. R. Nutt, The history of positron emission tomography. Mol. Imaging Biol. **4**, 11–26 (2002). https://doi.org/10.1016/S1095-0397(00)00051-0
4. G.T. Gullberg, G.L. Zeng, F.L. Datz et al., Review of convergent beam tomography in single photon emission computed tomography. Phys. Med. Biol. **37**, 507–534 (1992). https://doi.org/10.1088/0031-9155/37/3/002
5. J.L. Alberini, V. Edeline, A.L. Giraudet et al., Single photon emission tomography/computed tomography (SPET/CT) and positron emission tomography/computed tomography (PET/CT) to image cancer. J. Surg. Oncol. **103**, 602–606 (2011). https://doi.org/10.1002/jso.21695
6. World Nuclear Association, Radioisotopes in Medicine, https://world-nuclear.org/information-library/non-power-nuclear-applications/radioisotopes-research/radioisotopes-in-medicine.aspx. Accessed 7 Feb 2023
7. IAEA: IAEA Annual Report for 2021, https://www.iaea.org/opic/annual-report-2021
8. D. Habs, U. Köster, Production of medical radioisotopes with high specific activity in photonuclear reactions with γ-beams of high intensity and large brilliance. Appl. Phys. B **103**, 501–519 (2011). https://doi.org/10.1007/s00340-010-4278-1
9. B. Szpunar, C. Rangacharyulu, S. Date et al., Estimates of production of medical isotopes by photo-neutron reaction at the Canadian Light Source. Nucl. Instrum. Methods A **729**, 41–50 (2013). https://doi.org/10.1016/j.nima.2013.06.106
10. W. Luo, D.L. Balabanski, D. Filipescu, A data-based photonuclear simulation algorithm for determining specific activity of medical radioisotopes. Nucl. Sci. Tech. **27**, 5 (2016). https://doi.org/10.1007/s41365-016-0111-9
11. W. Luo, M. Bobeica, I. Gheorghe et al., Estimates for production of radioisotopes of medical interest at extreme light infrastructure-Nuclear physics facility. Appl. Phys. B **122**, 8 (2016). https://doi.org/10.1007/s00340-015-6292-9
12. W. Luo, Production of medical radioisotope ^{64} Cu by photoneutron reaction using ELI-NP γ-ray beam. Nucl. Sci. Tech. **27**, 96 (2016). https://doi.org/10.1007/s41365-016-0094-6
13. W.T. Pan, T. Song, H.Y. Lan et al., Photo-excitation production of medically interesting isomers using intense γ-ray source. Appl. Radiat. Isot. **168**, 109534 (2021). https://doi.org/10.1016/j.apradiso.2020.109534
14. H. Ejiri, T. Shima, S. Miyamoto et al., Resonant photonuclear reactions for isotope transmutation. J. Phys. Soc. Japan **80**, 094202 (2011). https://doi.org/10.1143/JPSJ.80.094202
15. J. Lee, H. Rehman, Y. Kim, A feasibility study on the transmutation of ^{100} Mo to ^{99m} Tc with laser-compton scattering photons. Nucl. Technol. **201**, 41–51 (2018). https://doi.org/10.1080/00295450.2017.1392397
16. H.Y. Lan, D. Wu, J.X. Liu et al., Photonuclear production of nuclear isomers using bremsstrahlung induced by laser-wakefield electrons. Nucl. Sci. Tech. **34**, 74 (2023). https://doi.org/10.1007/s41365-023-01219-x
17. IAEA(ed.) *Non-HEU Production Technologies for Molybdenum-99 and Technetium-99m* (IAEA, Vienna, 2013)
18. H.W. Wang, G.T. Fan, L.X. Liu et al., Commissioning of laser electron gamma beamline SLEGS at SSRF. Nucl. Sci. Tech. **33**, 87 (2022). https://doi.org/10.1007/s41365-022-01076-0
19. Z.R. Hao, G.T. Fan, H.W. Wang et al., Collimator system of SLEGS beamline at Shanghai Light Source. Nucl. Instr. Meth. A **1013**, 165638 (2021). https://doi.org/10.1016/j.nima.2021.165638
20. H.W. Wang, G.T. Fan, L.X. Liu et al., Development and prospect of Shanghai laser compton scattering gamma source. Nucl. Phys. Rev. **37**, 53–63 (2020)

21. Z.R. Hao, G.T. Fan, L.X. Liu et al., Design and simulation of a 4π ^{3}He fat efficiency neutron detector array. Nucl. Tech. **43**, 110501 (2020)
22. K.J. Chen, L.X. Liu, Z.R. Hao et al., Simulation and test of the SLEGS TOF spectrometer at SSRF. Nucl. Sci. Tech. **34**, 47 (2023). https://doi.org/10.1007/s41365-023-01194-3
23. P. Kuang, L.L. Song, K.J. Chen et al., Nuclear resonance fluorescence spectrometer design and detector performance analysis of Shanghai laser electron gamma source(SLEGS). Nucl. Phys. Rev. **40**, 58–65 (2023)
24. Y.X. Yang, Y. Zhang, W.J. Zhao et al., Construction of gamma activation experimental platform for Shanghai laser electron gamma source. Nucl. Phys. Rev. **31**, 1–6 (2023)
25. K. Goeke, J. Speth, Theory of giant resonances. Ann. Rev. Nucl. Part. Sci. **32**, 65–115 (1982). https://doi.org/10.1146/ANNUREV.NS.32.120182.000433
26. H. Feshbach, Unified Theory of Nuclear Reactions. Rev. Mod. Phys. **36**, 1076 (1964). https://doi.org/10.1103/RevModPhys.36.1076
27. M. Herman, G. Reffo, H.A. Weidenmüller, Multistep-compound contribution to precompound reaction cross section. Nucl. Phys. A **536**, 124–140 (1992). https://doi.org/10.1016/0375-9474(92)90249-J
28. L.Z. Dzhilavyan, A.I. Karev, V.G. Raevsky, Possibilities for the production of radioisotopes for nuclear-medicine problems by means of photonuclear reactions. Phys. Atom. Nuclei **74**, 1690–1696 (2011). https://doi.org/10.1134/S1063778811120040
29. M. Bobeica, D. Niculae, D. Balabanski et al., Radioisotopes production for medical applications at ELI-NP. Rom. Rep. Phys. **68**, S847–S883 (2016)
30. A. Zilges, D.L. Balabanski, J. Isaak et al., Photonuclear reactions-From basic research to applications. Prog. Part. Nucl. Phys. **122**, 103903 (2022). https://doi.org/10.1016/j.ppnp.2021.103903
31. D. Budker, J.C. Berengut, V.V. Flambaum et al., Expanding nuclear physics horizons with the gamma factory. Ann. Phys. **534**, 2100284 (2022). https://doi.org/10.1002/andp.202100284
32. Experimental Nuclear Reaction Data (EXFOR), https://www-nds.iaea.org/exfor/. Accessed 13 Feb 2023
33. NuDat 3 database, https://www.nndc.bnl.gov/nudat3/. Accessed 13 Feb 2023
34. R. Schwarzbach, K. Zimmermann, P. Bläuenstein et al., Development of a simple and selective separation of ^{67} Cufrom irradiated zinc for use in antibody labelling: A comparison of methods. Appl. Radiat. Isot. **46**, 329–336 (1995). https://doi.org/10.1016/0969-8043(95)00010-B
35. M. Yagi, K. Kondo, Preparation of carrier-free ^{47} Sc by the ^{48} Ti (γ, p). Int. J. Appl. Radiat. Isot. **28**, 463–468 (1977). https://doi.org/10.1016/0020-708X(77)90178-8
36. S.A. Kandil, B. Scholten, Z.A. Saleh et al., A comparative study on the separation of radiozirconium via ion-exchange and solvent extraction techniques, with particular reference to the production of ^{88} Zr and ^{89} Zr in proton induced reactions on yttrium. J. Radioanal. Nucl. Chem. **274**, 45–52 (2007). https://doi.org/10.1007/s10967-006-6892-2
37. B.L. Fèvre, C. Pin, A straightforward separation scheme for concomitant Lu-Hf and Sm-Nd isotope ratio and isotope dilution analysis. Anal. Chim. Acta **543**, 209–221 (2005). https://doi.org/10.1016/j.aca.2005.04.044
38. V.N. Starovoitova, L. Tchelidze, D.P. Wells, Production of medical radioisotopes with linear accelerators. Appl. Radiat. Isot. **85**, 39–44 (2014). https://doi.org/10.1016/j.apradiso.2013.11.122
39. M. Inagaki, S. Sekimoto, W. Tanaka et al., Production of ^{47} Sc, ^{67} Cu, ^{68} Ga, ^{105} Rh, ^{177} Lu, and ^{188} Re using electron linear accelerator. J. Radioanal. Nucl. Chem. **322**, 1703–1709 (2019). https://doi.org/10.1007/s10967-019-06904-z
40. A.G. Kazakov, T.Y. Ekatova, J.S. Babenya, Photonuclear production of medical radiometals: a review of experimental studies. J. Radioanal. Nucl. Chem. **328**, 493–505 (2021). https://doi.org/10.1007/s10967-021-07683-2
41. A. Koning, D. Rochman, Modern nuclear data evaluation with the TALYS code system. Nucl. Data Sheets **113**, 2841–2934 (2012). https://doi.org/10.1016/j.nds.2012.11.002
42. S. Stoulos, E. Vagena, Indirect measurement of bremsstrahlung photons and photoneutrons cross sections of ^{204} Pb and Sb isotopes compared with TALYS simulations. Nucl. Phys. A **980**, 1–14 (2018). https://doi.org/10.1016/j.nuclphysa.2018.09.081
43. P.V. Cuong, T.D. Thiep, L.T. Anh et al., Theoretical calculation by Talys code in combination with Geant4 simulation for consideration of (γ, n) reactions of Eu isotopes in the giant dipole resonance region. Nucl. Instrum. Methods B **479**, 68–73 (2020). https://doi.org/10.1016/j.nimb.2020.06.011
44. H. Cheng, B.H. Sun, L.H. Zhu et al., Measurements of ^{160} Dy (p, γ) at energies relevant for the astrophysical γ process. Astrophys. J. **915**, 78 (2021). https://doi.org/10.3847/1538-4357/ac00b1
45. W. Hauser, H. Feshbach, The inelastic scattering of neutrons. Phys. Rev. **87**, 366–373 (1952). https://doi.org/10.1103/PhysRev.87.366
46. A. Bockisch, Matched pairs for radionuclide-based imaging and therapy. Eur. J. Nucl. Med. Mol. Imaging **38**, 1–3 (2011). https://doi.org/10.1007/s00259-011-1780-6
47. S.M. Qaim, B. Scholten, B. Neumaier, New developments in the production of theranostic pairs of radionuclides. J. Radioanal. Nucl. Chem. **318**, 1493–1509 (2018). https://doi.org/10.1007/s10967-018-6238-x
48. H. Utsunomiya, S. Goriely, T. Kondo et al., Photoneutron cross sections for Mo isotopes: a step toward a unified understanding of (γ, n) and (n, γ) reactions. Phys. Rev. C **88**, 015805 (2013). https://doi.org/10.1103/PhysRevC.88.015805
49. R. Crasta, H. Naik, S.V. Suryanarayana et al., Photo-neutron cross-section of ^{100} Mo. J. Radioanal. Nucl. Chem. **290**, 367–373 (2011). https://doi.org/10.1007/s10967-011-1247-z
50. C.J. Anderson, R. Ferdani, Copper-64 radiopharmaceuticals for PET imaging of cancer: advances in preclinical and clinical research. Cancer Biother. Radiopharm. **24**, 379–393 (2009). https://doi.org/10.1089/cbr.2009.0674
51. J.Y. Kim, H. Park, J.C. Lee et al., A simple Cu-64 production and its application of Cu-64 ATSM. Appl. Radiat. Isot. **67**, 1190–1194 (2009). https://doi.org/10.1016/j.apradiso.2009.02.060
52. Q.H. Xie, H. Zhu, F. Wang et al., Establishing reliable Cu-64 production process: From target plating to molecular specific tumor micro-PET imaging. Molecules **22**, 641 (2017). https://doi.org/10.3390/molecules22040641
53. M. Jauregui-Osoro, S.D. Robertis, P. Halsted et al., Production of copper-64 using a hospital cyclotron: targetry, purification and quality analysis. Nucl. Med. Commun. **42**, 1024–1038 (2021). https://doi.org/10.1097/MNM.0000000000001422
54. L. Isolan, M. Malinconico, W. Tieu et al., A digital twin for ^{64} Cu production with cyclotron and solid target system. Sci. Rep. **12**, 19379 (2022). https://doi.org/10.1038/s41598-022-23048-5
55. L. Katz, A.G.W. Cameron, The solution of x-ray activation curves for photonuclear cross sections. Can. J. Phys. **29**, 518–544 (1951). https://doi.org/10.1139/p51-056
56. A.D. Antonov, N.P. Balabanov, Yu.P. Gangrsky et al., studied photonuclear reactions with the emission of α particles in the region of the Giant Dipole Resonance. Yad. Fiz. **51**, 305 (1990)

57. G.E. Coote, W.E. Turchinetz, I.F. Wright, Cross sections for the (γ, n) reaction in Cu^{63}, Cu^{65}, Zn^{64}, Sb^{121} and Pr^{141}, measured with monochromatic gamma rays. Nucl. Phys. **23**, 468–480 (1961). https://doi.org/10.1016/0029-5582(61)90273-5
58. S.M. Qaim, Therapeutic radionuclides and nuclear data. Radiochim. Acta **89**, 297–302 (2001). https://doi.org/10.1524/ract.2001.89.4-5.297
59. V. Starovoitova, D. Foote, J. Harris et al., Cu-67 photonuclear production. AIP Conf. Proc. **1336**, 502–504 (2011). https://doi.org/10.1063/1.3586150
60. D.A. Ehst, N.A. Smith, D.L. Bowers et al., Copper-67 production on electron linacs-Photonuclear technology development. AIP Conf. Proc. **1509**, 157–161 (2012). https://doi.org/10.1063/1.4773959
61. N.A. Smith, D.L. Bowers, D.A. Ehst, The production, separation, and use of ^{67} Cufor radioimmunotherapy: A review. Appl. Radiat. Isot. **70**, 2377–2383 (2012). https://doi.org/10.1016/j.apradiso.2012.07.009
62. R.A. Aliev, S.S. Belyshev, A.A. Kuznetsov et al., Photonuclear production and radiochemical separation of medically relevant radionuclides: ^{67} Cu. J. Radioanal. Nucl. Chem. **321**, 125–132 (2019). https://doi.org/10.1007/s10967-019-06576-9
63. G.H. Hovhannisyan, T.M. Bakhshiyan, R.K. Dallakyan, Photonuclear production of the medical isotope ^{67} Cu. Nucl. Instrum. Methods B **498**, 48–51 (2021). https://doi.org/10.1016/j.nimb.2021.04.016
64. N. Marceau, T.P.A. Kruck, D.B. McConnell et al., The production of copper 67 from natural zinc using a linear accelerator. Int. J. Appl. Radiat. Isot. **21**, 667–669 (1970). https://doi.org/10.1016/0020-708X(70)90121-3
65. A.K. Dasgupta, L.F. Mausner, S.C. Srivastava, A new separation procedure for ^{67} Cufrom proton irradiated Zn. Appl. Radiat. Isot. **42**, 371–376 (1991). https://doi.org/10.1016/0883-2889(91)90140-V
66. M.A. Hassanein, H. El-Said, M.A. El-Amir, Separation of carrier-free ^{64,67} Cu radionuclides from irradiated zinc targets using 6-tungstocerate(IV) gel matrix. J. Radioanal. Nucl. Chem. **269**, 75–80 (2006). https://doi.org/10.1007/s10967-006-0232-4
67. A.E. Sioufi, P. Erdos, P. Stoll, (γ, np) - Process in Mo-92 and Zn-66. Helv. Phys. Acta **30**, 264 (1957)
68. Y.W. Wang, D.Y. Chen, R.S. Augusto et al., Production review of accelerator-based medical isotopes. Molecules **27**, 5294 (2022). https://doi.org/10.3390/molecules27165294
69. P. Schaffer, F. Bénard, A. Bernstein et al., Direct production of ^{99m} Tc via ^{100} Mo $(p, 2n)$ on small medical cyclotrons. Phys. Procedia **66**, 383–395 (2015). https://doi.org/10.1016/j.phpro.2015.05.048
70. H.H. Xiong, Q.S. Zeng, Y.C. Han et al., Neutronics analysis of a subcritical blanket system driven by a gas dynamic trap-based fusion neutron source for ^{99} Mo production. Nucl. Sci. Tech. **34**, 49 (2023). https://doi.org/10.1007/s41365-023-01206-2
71. S. Sekimoto, K. Tatenuma, Y. Suzuki et al., Separation and purification of ^{99m} Tc from ^{99} Mo produced by electron linear accelerator. J. Radioanal. Nucl. Chem. **311**, 1361–1366 (2017). https://doi.org/10.1007/s10967-016-4959-2
72. NorthStar Medical Radioisotopes: Accelerator Mo-99 Production, https://www.northstarnm.com/development/accelerator-mo-99/. Accessed 15 Aug 2023
73. J.T. Harvey, G.H. Isensee, G.P. Messina et al., Domestic production of Mo99(2011), https://mo99.ne.anl.gov/2011/pdfs/Mo99/S7-P3_Harvey.pdf. Accessed 15 Aug 2023
74. B. Hesse, K. Tägil, A. Cuocolo et al., EANM/ESC procedural guidelines for myocardial perfusion imaging in nuclear cardiology. Eur. J. Nucl. Med. Mol. Imaging **32**, 855–897 (2005). https://doi.org/10.1007/s00259-005-1779-y
75. B.C. Cook, A.S. Penfold, V.L. Telegdi, Photodisintegration of C^{13}. Phys. Rev. **106**, 300–314 (1957). https://doi.org/10.1103/PhysRev.106.300
76. L.D. Cohen, W.E. Stephens, Gamma-ray activation of carbon. Phys. Rev. Lett. **2**, 263–264 (1959). https://doi.org/10.1103/PhysRevLett.2.263
77. J.P. Roalsvig, I.C. Gupta, R.N.H. Haslam, Photoneutron reactions in C^{12} and O^{16}. Can. J. Phys. **39**, 643–656 (1961). https://doi.org/10.1139/p61-075
78. W.E.D. Bianco, W.E. Stephens, Photonuclear activation by 20.5-MeV gamma rays. Phys. Rev. **126**, 709–717 (1962). https://doi.org/10.1103/PhysRev.126.709
79. E.B. Bazhanov, A.P. Komar, A.V. Kulikov et al., Photodisintegration of C^{12}. Yad. Fiz. **3**, 711 (1966)
80. B.C. Cook, J.E.E. Baglin, J.N. Bradford et al., $C^{12}(\gamma, n)$ C^{11} cross section to 65 MeV. Phys. Rev. **143**, 724–729 (1966). https://doi.org/10.1103/PhysRev.143.724
81. W.A. Lochstet, W.E. Stephens, ^{12} C $(\gamma, n)^{11}$ C giant resonance with gamma rays. Phys. Rev. **141**, 1002–1006 (1966). https://doi.org/10.1103/PhysRev.141.1002
82. J.D. King, R.N.H. Haslam, R.W. Parsons, The gamma-neutron cross section for N^{14}. Can. J. Phys. **38**, 231–239 (1960). https://doi.org/10.1139/p60-023
83. M.J. Facci, M.N. Thompson, The absolute ^{14} N (γ, n) reaction cross section. Nucl. Phys. A **465**, 77–82 (1987). https://doi.org/10.1016/0375-9474(87)90299-5
84. B.C. Cook, J.E.E. Baglin, J.N. Bradford et al., $O^{16}(\gamma, n)$ O^{15} cross section from threshold to 65 MeV. Phys. Rev. **143**, 712–723 (1966). https://doi.org/10.1103/PhysRev.143.712
85. B.S. Ishkhanov, I.M. Kapitonov, E.V. Lazutin et al., Fine structure of giant dipole resonance of the O^{16} nucleus. Yad. Fiz. **12**, 892 (1970)
86. S.N. Belyaev, A.B. Kozin, A.A. Nechkin et al., Photoabsorption cross sections of Pb, Bi, and Ta isotopes in the energy region $E_\gamma \leq 12$ MeV. Yad. Fiz. **42**, 1050 (1985)
87. S.N. Belyaev, V.A. Semenov, Intermediate structure in (γ, n) cross sections at nuclei with $N = 82$. Bull. Russ. Acad. Sci. Phys. **55**, 66 (1991)
88. P.R. Byerly, W.E. Stephens et al., Photodisintegration of copper. Phys. Rev. **83**, 54–62 (1951). https://doi.org/10.1103/PhysRev.83.54
89. A.I. Berman, K.L. Brown, Absolute cross section versus energy of the $Cu^{63}(\gamma, n)$ and $Cu^{63}(\gamma, 2n)$ reactions. Phys. Rev. **96**, 83–89 (1954). https://doi.org/10.1103/PhysRev.96.83
90. M.B. Scott, A.O. Hanson, D.W. Kerst, Electro- and photodisintegration cross sections of Cu^{63}. Phys. Rev. **100**, 209–214 (1954). https://doi.org/10.1103/PhysRev.100.209
91. T. Nakamura, K. Takamatsu, K. Fukunaga et al., Absolute cross sections of the (γ, n) reaction for Cu^{63}, Zn^{64}, and Ag^{109}. J. Phys. Soc. Japan **14**, 693–698 (1959). https://doi.org/10.1143/JPSJ.14.693
92. S. Yasumi, M. Yata, K. Takamatsu et al., Absolute cross section of the reaction $Cu^{63}(\gamma, n)$ Cu^{62} for Lithium gamma rays. J. Phys. Soc. Japan **15**, 1913–1919 (1960). https://doi.org/10.1143/JPSJ.15.1913
93. R.E. Sund, M.P. Baker, L.A. Kull et al., Measurements of the ^{63} Cu (γ, n) and $(\gamma, 2n)$ cross sections. Phys. Rev. **176**, 1366–1376 (1968). https://doi.org/10.1103/PhysRev.176.1366
94. D.G. Owen, E.G. Muirhead, B.M. Spicer, Structure in the giant resonance of ^{64} Zn and ^{63} Cu. Nucl. Phys. A **122**, 177–183 (1968). https://doi.org/10.1016/0375-9474(68)90711-2
95. L.Z. Dzhilavyan, N.P. Kucher, Measurement of the cross section of the reaction ^{63} Cu (γ, n) in a beam of quasimonochromatic

annihilation photons in the energy region 12–25 MeV. Yad. Fiz. **30**, 294 (1979)
96. S.C. Jeong, J.C. Kim, B.N. Sung, Cross section measurement for the ^{63} Cu $(\gamma, n)^{62}$ Cu reaction. J. Korean Phys. Soc. **17**, 359 (1984)
97. M.N. Martins, E. Hayward, G. Lamaze et al., Experimental test of the bremsstrahlung cross section. Phys. Rev. C **30**, 1855–1860 (1984). https://doi.org/10.1103/PhysRevC.30.1855
98. C. Plaisir, F. Hannachi, F. Gobet et al., Measurement of the ^{85} Rb $(\gamma, n)^{84m}$ Rb cross-section in the energy range 10–19 MeV with bremsstrahlung photons. Eur. Phys. J. A **48**, 68 (2012). https://doi.org/10.1140/epja/i2012-12068-7
99. K. Masumoto, T. Kato, N. Suzuki, Activation yield curves of photonuclear reactions for multielement photon activation analysis. Nucl. Instrum. Methods **157**, 567–577 (1978). https://doi.org/10.1016/0029-554X(78)90019-8
100. A.K.M.L. Rahman, K. Kato, H. Arima et al., Study on effective average (γ, n) cross section for ^{89} Y, ^{90} Zr, ^{93} Nb, and ^{133} Cs and $(\gamma, 3n)$ cross section for ^{99} Tc. J. Nucl. Sci. Technol. **47**, 618–625 (2010). https://doi.org/10.3327/jnst.47.618
101. A. Banu, E.G. Meekins, J.A. Silano et al., Photoneutron reaction cross section measurements on ^{94} Mo and ^{90} Zr relevant to the p-process nucleosynthesis. Phys. Rev. C **99**, 025802 (2019). https://doi.org/10.1103/PhysRevC.99.025802
102. T. Shizuma, H. Utsunomiya, P. Mohr et al., Photodisintegration cross section measurements on ^{186} W, ^{187} Re, and ^{188} Os: Implications for the Re-Os cosmochronology. Phys. Rev. C **72**, 025808 (2005). https://doi.org/10.1103/PhysRevC.72.025808
103. V.A. Zheltonozhsky, M.V. Zheltonozhskaya, A.M. Savrasov et al., Studying the activation of ^{177} Lu in (γ, pxn) reactions. Bull. Russ. Acad. Sci. Phys. **84**, 923–928 (2020). https://doi.org/10.3103/S1062873820080328
104. O.V. Bogdankevich, L.E. Lazareva, A.M. Moiseev, Inelastic scattering on ^{103} Rh nuclei. J. Exp. Theor. Phys. **12**, 853 (1961)
105. Z.M. Bigan, V.A. Zheltonozhsky, V.I. Kirishchuk et al., Excitation of ^{113} In, ^{195} Pt and ^{199} Hg isomers in reactions of inelastic gamma scattering. Bull. Russ. Acad. Sci. Phys. **70**, 292 (2006)
106. V.G. Nedorezov, E.S. Konobeevski, S.V. Zuyev et al., Excitation of ^{111m} Cd, ^{113m} In, and ^{115m} In isomeric states by photons of energy up to 8 MeV. Phys. Atom. Nucl. **80**, 827–830 (2017). https://doi.org/10.1134/S1063778817050167
107. O.V. Bogdankevich, L.E. Lazareva, F.A. Nikolaev, Inelastic scattering of photons by indium-115 nuclei. J. Exp. Theor. Phys. **4**, 320 (1957)
108. V.M. Mazur, I.V. Sokolyuk, Z.M. Bigan et al., Cross section for excitation of nuclear isomers in (γ, γ')-m reactions at 4–15 MeV. Yad. Fiz. **56**, 20 (1993)
109. N.A. Demekhina, A.S. Danagulyan, G.S. Karapetyan, Formation of isomeric states in (γ, γ') reactions at energies around the giant dipole resonance. Phys. Atom. Nucl. **64**, 1796–1798 (2001). https://doi.org/10.1134/1.1414927
110. V.S. Bokhinyuk, A.I. Guthy, A.M. Parlag et al., Study of the effective excitation cross section of the ^{115} In isomeric state in the (γ, γ') reaction. Ukr. J. Phys. **51**, 657 (2006)
111. W. Tornow, M. Bhike, S.W. Finch et al., Measurement of the ^{115} In $(\gamma, \gamma')^{115m}$ In inelastic scattering cross section in the 1.8 to 3.7 MeV energy range with monoenergetic photon beams. Phys. Rev. C **98**, 064305 (2018). https://doi.org/10.1103/PhysRevC.98.064305